ISSN 0915-633X

NATIONAL INSTITUTE FOR FUSION SCIENCE

Pair Creations of Negative and Positive Pionlike (Muonlike) Particle or K Mesonlike (Muonlike) Particle in H_2 or D_2 Gas Discharge in Magnetic Field

J. Uramoto

(Received - Oct. 14, 1997)

NIFS-532 Dec. 1997

RESEARCH REPORT
NIFS Series

NAGOYA, JAPAN

Pair Creations of Negative and Positive Pionlike (Muonlike) Particle or K Mesonlike (Muonlike) Particle in H_2 or D_2 gas discharge in magnetic field

Jōshin URAMOTO

National Institute for Fusion Science
332-6 Orosh-cho, Toki-shi, Gifu, 509-52, Japan

Abstract

Both negative pionlike (π^-) or muonlike (μ^-) particles and positive pionlike (π^+) or muonlike (μ^+) particles are extracted at an acceleration voltage of 800V with H^- ions and H^+, H_3^+ ions from outside region of H_2 gas discharge along magnetic field. Similarly, both negative K mesonlike (K^-) or muonlike (μ^-) particles and positive K mesonlike (K^+) or muonlike (μ^+) particles are extracted with D^- ions and D^+, (D_3^+) ions from outside region of D_2 gas discharge along magnetic field. Then, the π^-, μ^-, K^- particles are detected easily as the apparent current to the beam collector (BC) of a magnetic mass analyzer increases extremely when a positive bias voltage is applied to BC and positive ions are supplied in front of BC. It should be noted that the π^+, μ^+, K^+ particles do not penetrate a metal plate while the π^-, μ^-, K^- particles penetrate the metal plate easily.

Keywords: positive pionlike particle π^+, positive muonlike particle μ^+, positive K mesonlike particle K^+.

1. Introduction

It has been reported already[1),2),3)] that negative pionlike (π^-), muonlike (μ^-) and K mesonlike (K^-) particles are extracted from the outside region of the H_2 or D_2 gas discharge in magnetic fields, and that a special detection method[4)] for their particles is necessary.

Similarly, it has been reported[5),6)] also that the π^- or μ^- particles are produced under a different production method using an electron beam and positive ion beam. Recently, under this method, we find[7)] that both negative pionlike (π^-) or muonlike (μ^-) particles and positive pionlike (π^+) or muonlike particles (μ^+) are produced as a pair creation.

In this paper, we will investigate a similar pair creation like the π^- and π^+ particles under a H_2 or D_2 gas discharge in magnetic fields.

2. Detections of H^-, π^-, μ^-

Schematic diagrams of the experimental apparatus are shown in Figs. 1. The apparatus is constructed from a H_2 gas discharge plasma in magnetic fields, three extraction electrodes (with an aperture of 3 mm in diameter) to extract some negatively charged particles and a magnetic mass analyzer (90° deflection-type).

A sheet plasma[8),9),10)] is produced to generate H^- ions effectively and in wide area. That is, the discharge (cylindrical) plasma flow of about 1 cm in diameter is transformed into a sheet plasma flow of about 3 mm in thickness and about 20 cm in width. The sheet plasma flow enters the anode through the main chamber (50 cm long). A uniform magnetic field of about 50 gauss is applied along the sheet plasma flow in the main chamber where the H_2 gas pressure is about 1.5×10^{-3} Torr. The anode current I_A is 20A. A distance between the sheet plasma center and the first extraction electrode (L) is 7.5 cm. The plasma density in the center of the sheet plasma is about 10^{11}/cc and the electron temperature is about 20 eV. The positive ion density in front of the first extraction electrode is estimated to be about 10^{10}/cc from a positive ion saturation current as H_3^+, while the electron density from the Langmuir probe characteristic is about 10^9/cc and the electron temperature is about 3.0 eV. That is, the electron density in front of the first extraction electrode is reduced near 1/10 of the positive ion density.

The negatively charged particles extracted from the H_2 gas discharge plasma, are injected into the ordinary magnetic mass analyzer (MA) through the slit (3 mm × 1 cm) while each mass of the

negatively charged particle is estimated by the following relations: From the analyzing magnetic field B_M where the negative current to the beam collector BC shows a peak, the curvature radius r of the mass analyzer and the extraction (acceleration) voltage V_E, we can estimate the mass m of the negatively charged particle by,

$$m = \frac{Ze\,(B_M r)^2}{2V_E}$$

$$= \frac{8.8 \times 10^{-2}\, Z\,(B_M r)^2\, m_e}{V_E}, \quad \cdots\cdots (1)$$

where e is the electron charge, B_M is in gauss unit, r is in cm unit, V_E is in volt unit and m_e is the electron mass and Z is the charge number. For the curvature radius $r = 4.3$ cm of this mass analyzer, the Eq. (1) is rewritten by

$$m = \frac{1.63\, Z\, B_M{}^2}{V_E} m_e. \quad \cdots\cdots (2)$$

In the extraction of negatively charged particles, the first extraction electrode (L) is electrically floated, whose potential V_L is about −10V with respect to the anode (11). A potential V_M of the second extraction electrode (M) is kept at 100V. A potential V_E of the final extraction electrode (E) is 800V.

In this experiment, it is noted that the back space of the beam collector is shielded[4] perfectly from the diffusion of positive ions as shown in Fig. 1 (B). The dependences of the negative current I^- to the beam collector on the analyzing magnetic field B_M are shown in Fig. 2 for the beam collector potential $V_{BC} = 0$V and $V_{BC} = 100$V. Obviously, in a case (1) of Fig. 2, a main peak of I^- at the analyzing magnetic field $B_M \approx (4.0 \times 240)$ gauss = 960 gauss is corresponding to H^- ion, assuming that Z = 1 in Eq. (2). That is, we obtain $m \approx 1880\, m_e$ (near the true mass of $H^- = 1842\, m_e$) as $V_E = 800$V. Then, we find that the middle peak of I^- at $B_M \approx (1.54 \times 240)$ gauss ≈ 370 gauss is corresponding to a negative pion, assuming that Z = 1 in Eq. (2). That is, we obtain $m \approx 278\, m_e$ (near the true pion mass = $273\, m_e$) as $V_E = 800$V.

Similarly, we find that the first peak of I^- at $B_M \approx (1.33 \times 240)$ gauss = 320 gauss is corresponding to a negative muon, assuming that Z = 1 in Eq. (2). That is, we obtain $m = 209\, m_e$ (near

the true muon mass = 207 m_e) as V_E = 800V.

When a positive potential V_{BC} = 100V is applied to the beam collector BC, their peaks of I^- increase, as seen in a case (2), about 1.3 times for H^- ion, about 300 times of π^- or μ^-. These large apparent increments of negative current peaks under the positive bias potential $V_{BC} > 0$ of the beam collector BC, can be explained from assistance of positive ions in front of BC[7),11)].

3. Detections of H^+ (H_3^+), π^+, μ^+

Schematic diagrams of the experimental apparatus are shown in Figs. 3. The apparatus is constructed from the same H_2 gas discharge plasma with the case of H^-, π^-, μ^- in Figs. 1, three extraction electrodes to extract some "positively" charged particles and the mass analyzer where the polarity of analyzing magnetic field B_M is reversed (to $-B_M$).

The positively charged particles extracted from the H_2 gas discharge plasma, are injected into the magnetic mass analyzer (MA) while each mass of the positively charged particles is estimated by the same relations of Eq. (1) and Eq. (2) with the case of H^-, π^-, μ^-. In the extraction of positively charged particles, the first extraction electrode (L) is electrically floated, whose potential V_L is about –10V with respect to the discharge anode. A potential V_M of the second extraction electrode (M) is –100V and a potential V_E of the final extraction electrode (E) in –800V.

The dependences of the positive current I^+ to BC on $(-B_M)$ are shown in Fig. 4 for the beam collector potential V_{BC} = 0V. Obviously, in Fig. 4, a large peak of I^+ at $-B_M \approx (4.0 \times 240)$ gauss = 960 gauss is corresponding to H^+ ion, assuming that Z = 1 in Eq. (2). That is, we obtain m ≈ 1880 m_e as $|V_E|$ = 800V. Another large peak of I^+ at $-B_M \approx (6.8 \times 240)$ gauss ≈ 1630 gauss is corresponding to H_3^+ ion, assuming that Z = 1 in Eq. (2). That is, we obtain m ≈ 5420 m_e.

Next, two small peaks of I^+ to BC are seen in Fig. 4. We find that the first peak at $-B_M \approx (1.35 \times 240)$ gauss ≈ 324 gauss is corresponding to a positive muonlike (μ^+) particle and the second peak at $-B_M \approx (1.60 \times 240)$ gauss ≈ 384 gauss is corresponding to a positive pionlike (π^+) particle, assuming that Z = 1 in Eq. (2). That is, we obtain m ≈ 210 m_e (near the true muon mass 207 m_e) for the first peak and m ≈ 300 m_e (near the true pion mass 273 m_e) for the second peak.

In these detections of the positively charged particles, even if the bias potential V_{BC} of BC is varied from 100V to –100V, the peak currents of I^+ are not varied. That is, no apparent current increments are observed in comparison with the cases of the negatively charged particles.

Thus, we conclude that a pair creation of π^- (μ^-) and π^+ (μ^+) particle is arised outside of the H_2 gas discharge plasma in magnetic fields and that the π^- and μ^- particles are detected easily as the apparent current to BC of MA increases extremely when positive bias voltage is applied to BC and positive ions are supplied in front of BC through reflection of H^- ions as shown in Fig. 1 (B).

4. Comparison with He gas discharge

In the experimental apparatus of Figs. 1 and Figs. 3, a He gas was introduced instead of H_2 gas and a He gas discharge was fired at a discharge current of 15A in a pressure of 2.3×10^{-3} Torr. The plasma density in the sheet plasma was about 10^{11}/cc and the electron temperature was about 25 eV. The plasma density in front of the first extraction electrode was about 1.5×10^{10}/cc and the electron temperature was about 3.5 eV.

The dependences of the negative current I^- to the beam collector (BC) on the analyzing magnetic field (B_M) are shown in Fig. 5 under the bias voltages of BC $V_{BC} = 0V$ and $V_{BC} = 100V$. Then, I^- peaks of He^- ion are not seen while a very small I^- peak of H^- ion and two very small I^- peaks of π^- and μ^- particle appear. Obviously, these small peaks of I^- are generated by a very small amount of H_2 gas which is mixed in the main He gas.

Next, the dependences of the positive current I^+ to BC on the reversed magnetic field ($-B_M$) are shown in Fig. 6. A main I^+ peak of H^+ ion (accelerated at 800V) is seen while a small I^+ peak of H^+ ion and two extremely small I^+ peaks of π^+ and μ^+ particles appear. Similarly, these small I^+ peaks are generated by the very small amount of H_2 gas.

5. Detections of D^-, K^-, μ^-

A schematic diagram of the experimental apparatus is shown in Fig. 1. The apparatus is constructed from a D_2 gas discharge plasma in magnetic fields, three extraction electrodes (with an aperture of 3 mm in diameter) to extract some negatively charged particles and a magnetic mass analyzer (90° deflection-type).

A sheet plasma[10] is produced to generate D^- ions effectively and in wide area. That is, the discharge (cylindrical) plasma flow of about 1 cm in diameter is transformed into a sheet plasma flow of about 3 mm in thickness and about 20 cm in width. The sheet plasma flow enters the anode through the main chamber (50 cm long). A uniform magnetic field of about 50 gauss is

applied along the sheet plasma flow in the main chamber where the D_2 gas pressure is about 1.5×10^{-3} Torr. The discharge anode current I_A is 20A. A distance between the sheet plasma center and the first extraction electrode (L) is 7.5 cm. The plasma density in the center of the sheet plasma is about 10^{11}/cc and the electron temperature is about 20 eV. The positive ion density in front of the first extraction electrode is estimated to be about 10^{10}/cc from a positive ion saturation current as D_3^+, while the electron density from the Langmuir probe characteristic is about 10^9/cc and the electron temperature is about 3.0 eV. That is, the electron density in front of the first extraction electrode is reduced near 1/10 of the positive ion density.

The negatively charged particles extracted from the D_2 gas discharge plasma, are injected into the ordinary magnetic mass analyzer (MA) through the slit (3 mm × 1 cm) while each mass of the negatively charged particle is estimated by the following relations: From the analyzing magnetic field B_M where the negative current to the beam collector BC shows a peak, the curvature radius r of the mass analyzer and the extraction (acceleration) voltage V_E, we can estimated the mass m of the negatively charged particle by,

$$m = \frac{Ze\,(B_M r)^2}{2V_E}$$

$$= \frac{8.8 \times 10^{-2}\, Z\,(B_M r)^2\, m_e}{V_E}, \quad \cdots\cdots (1)$$

where e is the electron charge, B_M is in gauss unit, r is in cm unit, V_E is in volt unit and m_e is the electron mass and Z is the charge number. For the curvature radius $r = 4.3$ cm of this mass analyzer, the Eq. (1) is rewritten by

$$m = \frac{1.63\, Z\, B_M{}^2}{V_E} m_e. \quad \cdots\cdots (2)$$

In the extraction of negatively charged particles, the first extraction electrode (L) is electrically floated, whose potential V_L is about −10V with respect to the anode. A potential V_M of the second extraction electrode (M) is 100V. A potential V_E of the final extraction electrode (E) is 800V.

A result of the mass analysis for extraction of negatively charged particles from the D_2 gas discharge plasma, is shown in Fig. 8. Dependences of the negative current I^- to the beam collector

BC on the analyzing magnetic field B_M are shown, where the bias voltage V_{BC} of BC with respect to the mass analyzer, is $V_{BC} = 0V$ and $V_{BC} = 300V$.

In a case (1) of Fig. 8, a main peak of I^- at the analyzing magnetic field $B_M \approx (5.6 \times 240)$ gauss = 1344 gauss is corresponding to D^- ion, assuming that Z = 1 in Eq. (2). That is, we obtain $m \approx 3685\ m_e$ (near the true mass of $D^- = 3683\ m_e$) as $V_E = 800V$. Then, we find that the middle peak of I^- at $B_M \approx (2.8 \times 240)$ gauss = 672 gauss is corresponding to a negative K meson (K^-), assuming that Z = 1 in Eq. (2). That is, we obtain $m \approx 921\ m_e$ (near the true K^- mass $\approx 966\ m_e$). Similarly, we find that the first peak of I^- at $B_M \approx (1.35 \times 240)$ gauss = 324 gauss is corresponding to a negative muon (μ^-), assuming that Z = 1 in Eq. (2). That is, we obtain $m \approx 214\ m_e$ (near the true muon mass = 207 m_e). When a positive bias potential $V_{BC} = 300V$ is applied to BC, their peaks of I^- increase , as seen in a case (2), about 1.4 times for D^- ion, about 250 times for K^- or μ^-. These large apparent increments of I^- peaks under the positive bias potential $V_{BC} > 0$ of BC have been explained already[8], which are due to the same mechanism with that in the case of H_2 gas discharge.

6. Detections of D^+ (D_3^+), K^+, μ^+

Schematic diagrams of the experimental apparatus are shown in Figs. 9. The apparatus is constructed from the same D_2 gas discharge plasma with the case of D^-, K^-, μ^- in Fig. 7, three extraction electrodes to extract some "positively" charged particles and the mass analyzer where the polarity of analyzing magnetic field B_M is reversed (to $-B_M$).

The positively charged particles extracted from the D_2 gas discharge plasma, are injected into the magnetic mass analyzer (MA) while each mass of the positively charged particles is estimated by the same relations of Eq. (1) and Eq. (2) with the case of D^-, K^-, μ^-. In the extraction of positively charged particles, the first extraction electrode (L) is electrically floated, whose potential V_L is about −10V with respect to the discharge anode. A potential V_M of the second extraction electrode (M) is −100V and a potential V_E of the final extraction electrode (E) in −800V.

The dependences of the positive current I^+ to BC on ($-B_M$) are shown in Fig. 10 for the beam collector potential $V_{BC} = 0V$. Obviously, in Fig. 10, a large peak of I^+ at $-B_M \approx (5.6 \times 240)$ gauss = 960 gauss is corresponding to D^+ ion, assuming that Z = 1 in Eq. (2). That is, we obtain $m \approx 3685\ m_e$ (near the true mass of $D^+ = 3681\ m_e$). Here, another large peak of I^+ corresponding to

D_3^+ is neglected under an upper limit of the magnetic field intensity of MA.

Next, two small peaks of I^+ to BC are seen in Fig. 10. We find that the first peak at $-B_M \approx (1.35 \times 240)$ gauss ≈ 324 gauss is corresponding to a positive muonlike (μ^+) particle and the second peak at $-B_M \approx (2.8 \times 240)$ gauss ≈ 672 gauss is corresponding to a positive K meson (K^-), assuming that $Z = 1$ in Eq. (2). That is, we obtain $m \approx 921\ m_e$ (near the true K^+ mass $\approx 966\ m_e$).

In these detection, even if the bias potential V_{BC} of BC is varied from 300V to –300V, the peak currents I^+ are not varied almost. That is, no apparent current increments are observed.

Thus, we conclude that a pair creation of K^- (μ^-) and K^+ (μ^+) particle is arised outside of the D_2 gas discharge plasma in magnetic fields and that the K^- and μ^- particles are detected easily as the apparent current to BC of MA increases extremely under $V_{BC} > 0$ and assistance of D^+ ions.

7. Difference of Metal Plate Penetration between Negative Particles and Positive Particles

Penetrations of metal plate for the negative particles (H^-, π^-, μ^-) and the positive particles (H^+, H_3^+, π^+, μ^+) are investigated by arranging a metal plate (MP) of 1 mm in thickness in front of the beam collector (BC) as shown in Figs. 11 and Figs. 12. The dependences of I^- or I^+ current to BC on B_M or $-B_M$ are shown in Fig. 13. In comparison with those of Fig. 2 and Fig. 4, the π^- and μ^- particles penetrate the metal plate MP (above 1/2) while the H^- ions, the H^+, H_3^+ ions and the π^+, μ^+ particles do not penetrate it. It is natural that the classical H^-, H^+, H_3^+ ions can not penetrate the MP in this low energy of 800 eV. However, it is a very important discovery that the π^+, μ^+ particles can not penetrate the MP while the π^-, μ^- particles in this low energy penetrate it.

Next, in the D_2 gas discharge plasma as shown in Figs. 9, similar penetrations for the negative particles (D^-, K^-, μ^-) and the positive particles (D^+, K^+, μ^+) are investigated under the similar apparatus to that as shown in Figs. 11 and Fig. 12.

The dependences of I^- or I^+ current to BC on B_M or $-B_M$ are shown in Fig. 14. In comparison with those of Fig. 8 and Fig. 10, the K^- and μ^- particles penetrate the MP (above 1/2) while the D^- ions, the D^+, (D_3^+) ions and the K^+, μ^+ particles do not penetrate it. These experimental results are similar to those in the case of the H_2 gas discharge.

References

1) J. Uramoto: National Institute of Fusion Science, Nagoya, Japan-Research Report, NIFS-377 (1995).

2) J. Uramoto: NIFS-418 (1996).

3) J. Uramoto: NIFS-414 (1996).

4) J. Uramoto: NIFS-400 (1996).

5) J. Uramoto: NIFS-266 (1993).

6) J. Uramoto: NIFS-277 (1994).

7) J. Uramoto: NIFS- To be reported.

8) J. Uramoto: Journal of the vacuum society of Japan, **25** (1982) 719 in Japanese.

9) J. Uramoto: Journal of the vacuum society of Japan, **27** (1984) 600 in Japanese.

10) J. Uramoto: Journal of the vacuum society of Japan, **27** (1984) 610.

11) J. Uramoto: To be reported.

Figure Captions

Fig. 1 (A) Schematic diagram of experimental apparatus for negative particle detection under H_2 gas discharge.

1: Cylindrical plasma in discharge anode. 2: Discharge cathode. 3: H_2 gas flow. 4: Discharge power supply. 5: Electron acceleration power supply. 6: Vacuum pump. 7: Area where cylindrical plasma is transformed into sheet plasma. 8: Insulation tube. 9: A pair of permanent magnets. 10: Magnetic field coils. 11: Anode. I_A: Current to anode. CP: Cylindrical plasma. SP: Sheet plasma. B_Z: Magnetic field. L: First extraction electrode. M: Second extraction electrode. E: Final extraction electrode. V_M: Potential (100V) of second extraction electrode with respect to anode. V_E: Potential (800V) of final extraction electrode with respect to anode. MA: Magnetic deflection (90°) mass analyzer. B_M: Magnetic field intensity of MA. BC: Beam collector of MA. V_{BC}: Positive potential of BC with respect to MA. I^-: Negative current to BC. $H\bar{0}$: Hydrogen negative ions outside of sheet plasma. H^-: Accelerated hydrogen negative ions. $\pi\bar{0}$: Negative pionlike particles outside of sheet plasma. π^-: Accelerated negative pionlike particles.

Fig. 1 (B) Schematic diagram of mass analyzer for negative particle detection.

S: Entrance slit position. X: Entrance of uniform magnetic field.

Ins: Insulator behind BC. + Ion: Positive ions in front of BC. Fe: shows Iron.

Fig. 2 (1) Dependences of negative current I^- to BC on magnetic field B_M of MA under (1) beam collector potential $V_{BC} = 0V$ and (2) $V_{BC} = 100V$.

H^-: Peak of I^- corresponding to H^- ion. π^-: Peak of I^- corresponding to negative pionlike particle. μ^-: Peak of I^- corresponding to negative muonlike particle.

Fig. 3 (A) Schematic diagram of experimental apparatus for positive particle detection under H_2 gas discharge.

V_M: −100V. V_E: −800V. I^+: Positive current to BC. H_0^+: Hydrogen positive ions outside of sheet plasma. H^+: Accelerated hydrogen positive ions. $\pi\bar{0}^+$: Positive pionlike particles outside of sheet plasma. π^+: Accelerated pionlike particles.

(See captions of Fig. 1).

Fig. 3 (B) Schematic diagram of mass analyzer for positive particle detection.

$-B_M$: Reversed magnetic field of MA.

Fig. 4 Dependences of positive current I^+ to BC on reversed magnetic field ($-B_M$) of MA under beam collector bias voltage $V_{BC} = 0 \sim \pm 100V$.

π^+: Peak of I^+ corresponding to positive pionlike particle. μ^+: Peak of I^+ corresponding to positive muonlike particle. H^+ or H_3^+: Peak of I^+ corresponding to H^+ or H_3^+ ion.

Fig. 5 Mass analysis under He gas discharge by the experimental apparatus of Fig. 1. Dependences of negative current I^- to BC on B_M under (1) $V_{BC} = 0V$ and (2) $V_{BC} = 100V$.

H^-: H^- ion. π^-: Negative pionlike particle. μ^-: Negative muonlike particle.

*(H^-, π^-, μ^-) are produced by a small amount of H_2 gas mixing in the main He gas.

Fig. 6 Mass analysis under He gas discharge by the experimental apparatus of Fig. 3. Dependences of positive current I^+ to BC on ($-B_M$) under $V_{BC} = 0 \sim \pm 100V$.

He^+: Peak of I^+ corresponding to He^+ ion. H^+: H^+ ion. π^+: Positive pionlike particle. μ^+: Positive muonlike particle.

*(H^+, π^+, μ^+) are produced by H_2 gas mixing in the main He gas.

Figs. 7 (A) and (B) Schematic diagrams of experimental apparatus for negative particle detection under D_2 gas discharge.

3: D_2 gas flow. D_0^-: Deuterium negative ions outside of sheet plasma. D^-: Accelerated deuterium negative ions. K_0^-: negative K mesonlike particles outside of sheet plasma. K^-: Accelerated K mesonlike particles.

(See captions of Fig. 1).

Fig. 8 Dependences of negative current I^- to BC on B_M under (1) $V_{BC} = 0V$ and (2) $V_{BC} = 300V$.

D^-: Peak of I^- corresponding to D^- ion. K^-: Peak of I^- corresponding to negative K mesonlike particle. μ^-: Peak of I^- corresponding to negative muonlike particle.

Figs. 9 (A) and (B) Schematic diagrams of experimental apparatus for positive particle detection under D_2 gas discharge.

3: D_2 gas flow. $V_M = -100V$. $V_E = -800V$. I^+: Positive current to BC. D_0^+: Deuterium positive ions outside of sheet plasma. D^+: Accelerated deuterium positive ions. K_0^+: Positive K mesonlike particles outside of sheet plasma. K^+: Accelerated K mesonlike particles.

(See captions of Fig. 1 and Fig. 3).

Fig. 10 Dependences of positive current I^+ to BC on reversed magnetic field ($-B_M$) under $V_{BC} = 0 \sim \pm 300V$.

D^+: Peak of I^+ corresponding to D^+ ion. K^+: Peak of I^+ corresponding to positive K mesonlike particle. μ^+: Peak of I^+ corresponding to negative muonlike particle.

Fig. 11 (A) Schematic diagrams of mass analyzer MA for metal plate penetration of negative particles.

MP: Metal plate (1 mm in thickness).

(See captions of Fig. 1).

Fig. 11 (B) Another schematic diagram of mass analyzer.

MA: Mass analyzer. C: Magnetic coil. Fe: Iron. (N): North pole of electro-magnet. (S): South pole. B_M: Analyzing magnetic field.

(See captions of Fig. 1).

Fig. 12 (A) Schematic diagrams of mass analyzer MA with the reversed analyzing magnetic field for metal plate penetration of positive particles.

MP: Metal plate. ($-B_M$): Reversed analyzing magnetic field.

Fig. 12 (B) Another schematic diagram of MA with ($-B_M$).

(See captions of Fig. 1).

Fig. 13 Dependences of I^- or (I^+) to BC on B_M or ($-B_M$) under H_2 gas discharge (in the case where a metal plate MP is arranged as shown in Fig. 11 or 12).

(1): $V_{BC} = 0V$. (2) $V_{BC} = 100V$. π^-: Negative pionlike particles which penetrate MP. μ^-: Negative muonlike particles which penetrate MP.

Fig. 14 Dependences of I^- or (I^+) to BC on B_M or ($-B_M$) under D_2 gas discharge (in the case where MP is arranged as shown in Fig. 11 or 12).

(1): $V_{BC} = 0V$. (2) $V_{BC} = 300V$. K^-: Negative K mesonlike particles which penetrate MP. μ^-: Negative muonlike particles which penetrate MP.

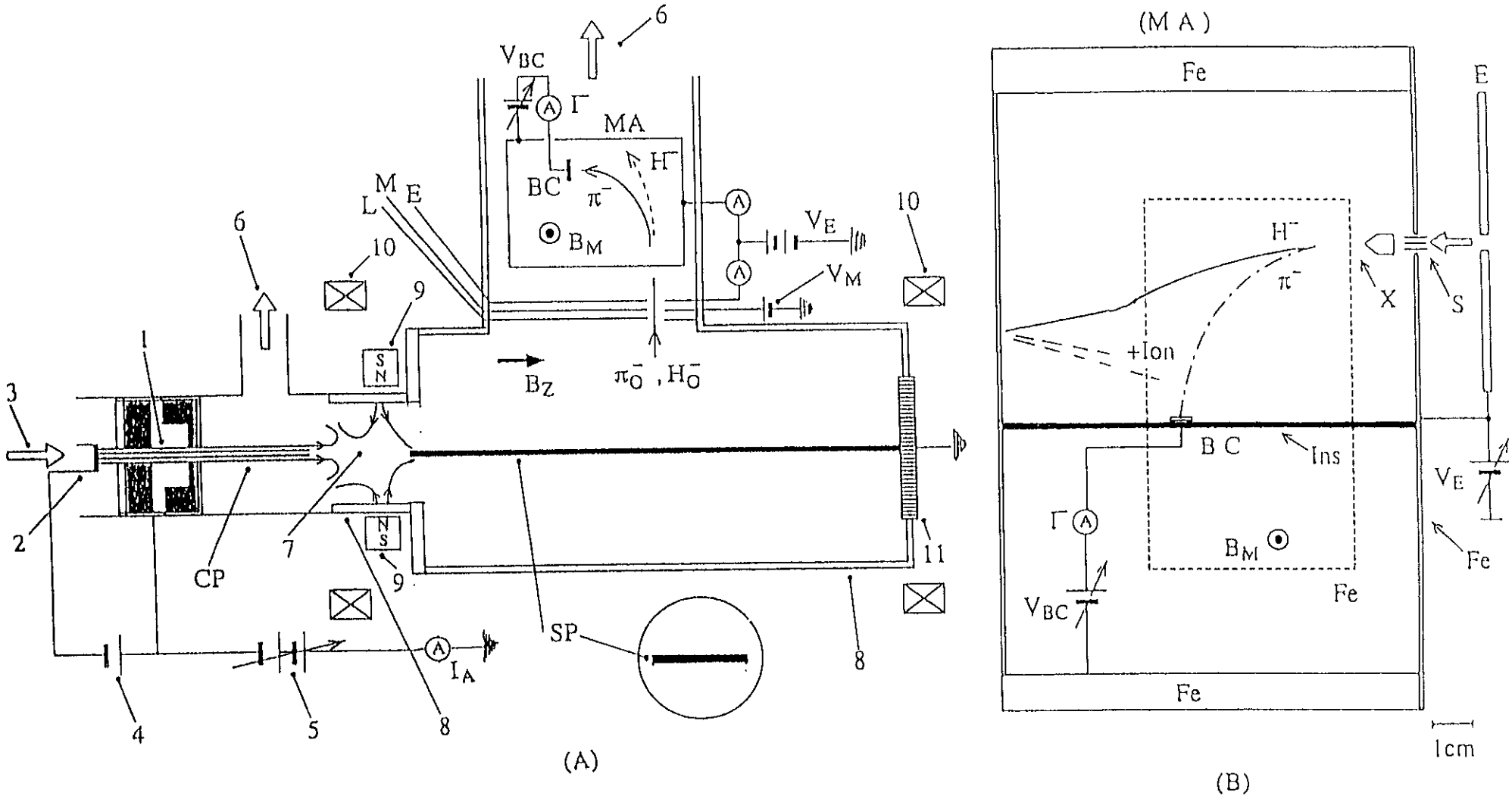
6
V_{BC}
Γ
MA
BC
H^-
π^-
B_M
L
M
E
V_E
V_M
10
9
B_Z
π_0^- , H_0^-
3
1
2
CP
7
SP
11
8
4
5
I_A
(A)
(M A)
Fe
E
+Ion
X
S
B C
Ins
V_E
Fe
B_M
V_{BC}
1cm
(B)

Fig. 1

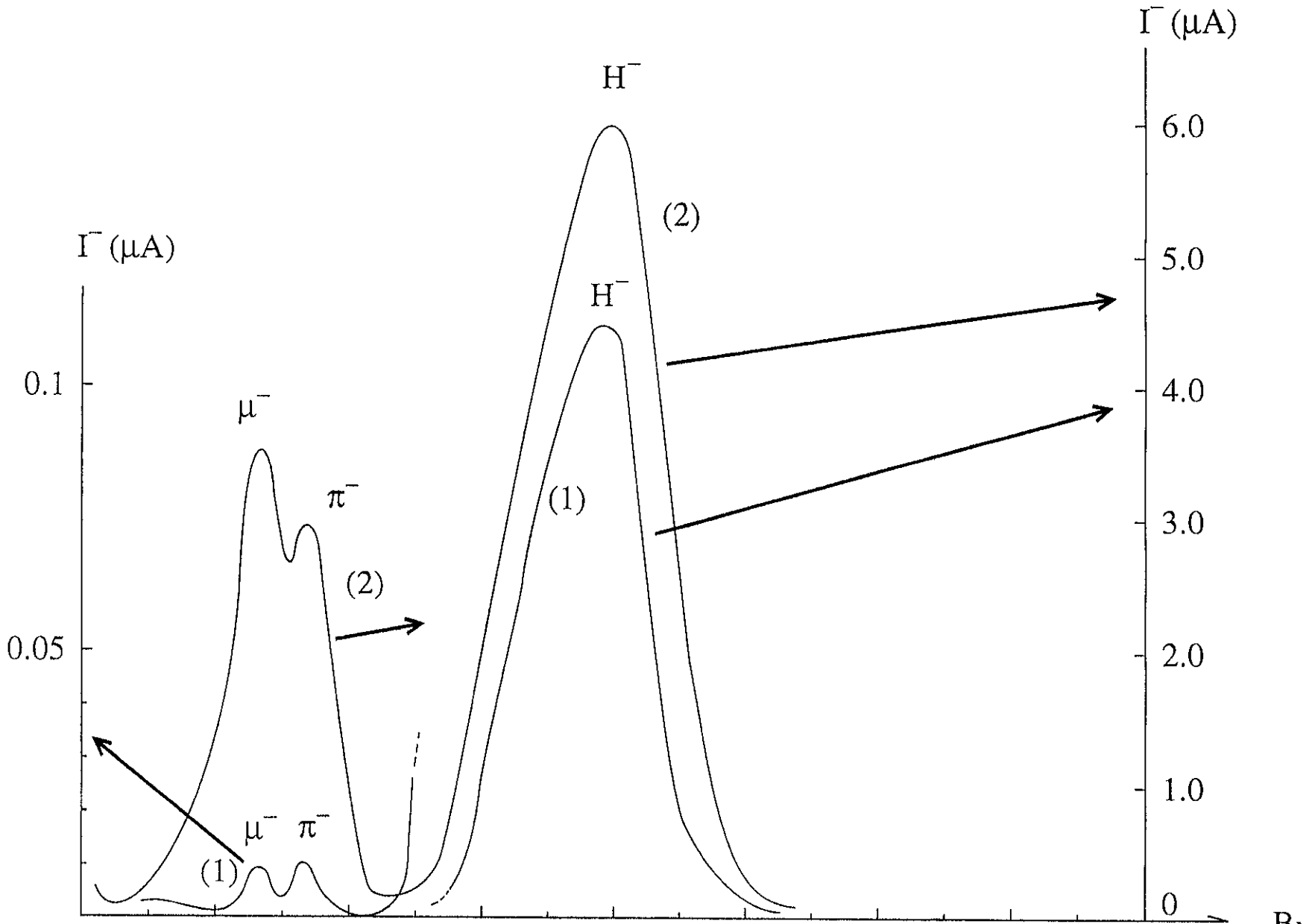
I⁻ (μA)
H⁻
(2)
H⁻
I⁻ (μA)
0.1
μ⁻
π⁻
(2)
(1)
0.05
μ⁻ π⁻
(1)
0
1.0
2.0
3.0
4.0
5.0
6.0
7.0
8.0
(×240 Gauss)
I⁻ (μA)
6.0
5.0
4.0
3.0
2.0
1.0
0
BM

Fig. 2

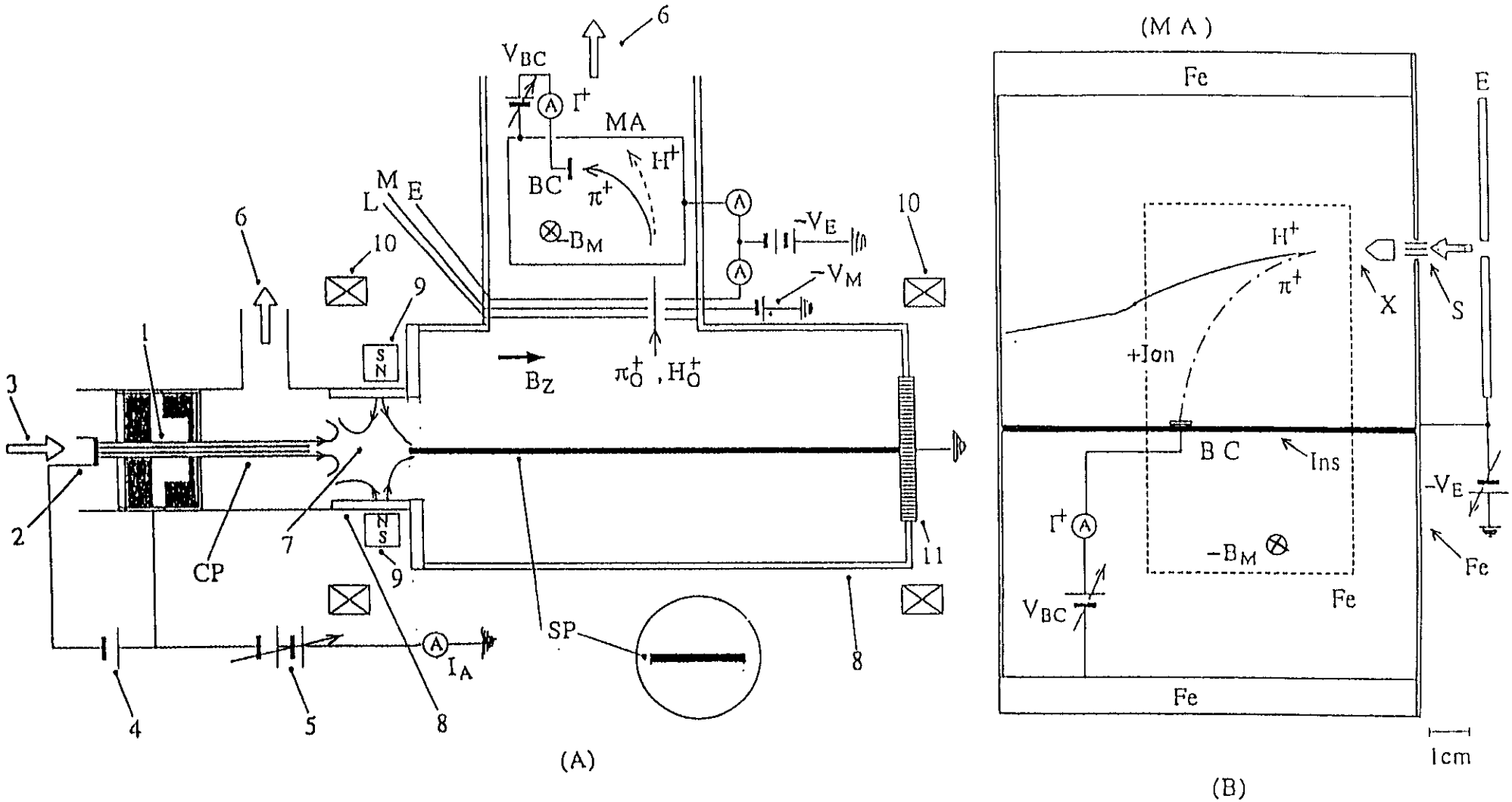
6
V_{BC}
I^+
MA
H^+
BC
π^+
B_M
M
L
E
$-V_E$
$-V_M$
10
9
B_Z
π_0^+ , H_0^+
1
3
2
CP
7
11
SP
8
I_A
4
5
(A)
(M A)
Fe
E
H^+
π^+
X
S
+Ion
B C
Ins
$-V_E$
I^+
$-B_M$
V_{BC}
Fe
1cm
(B)

Fig. 3

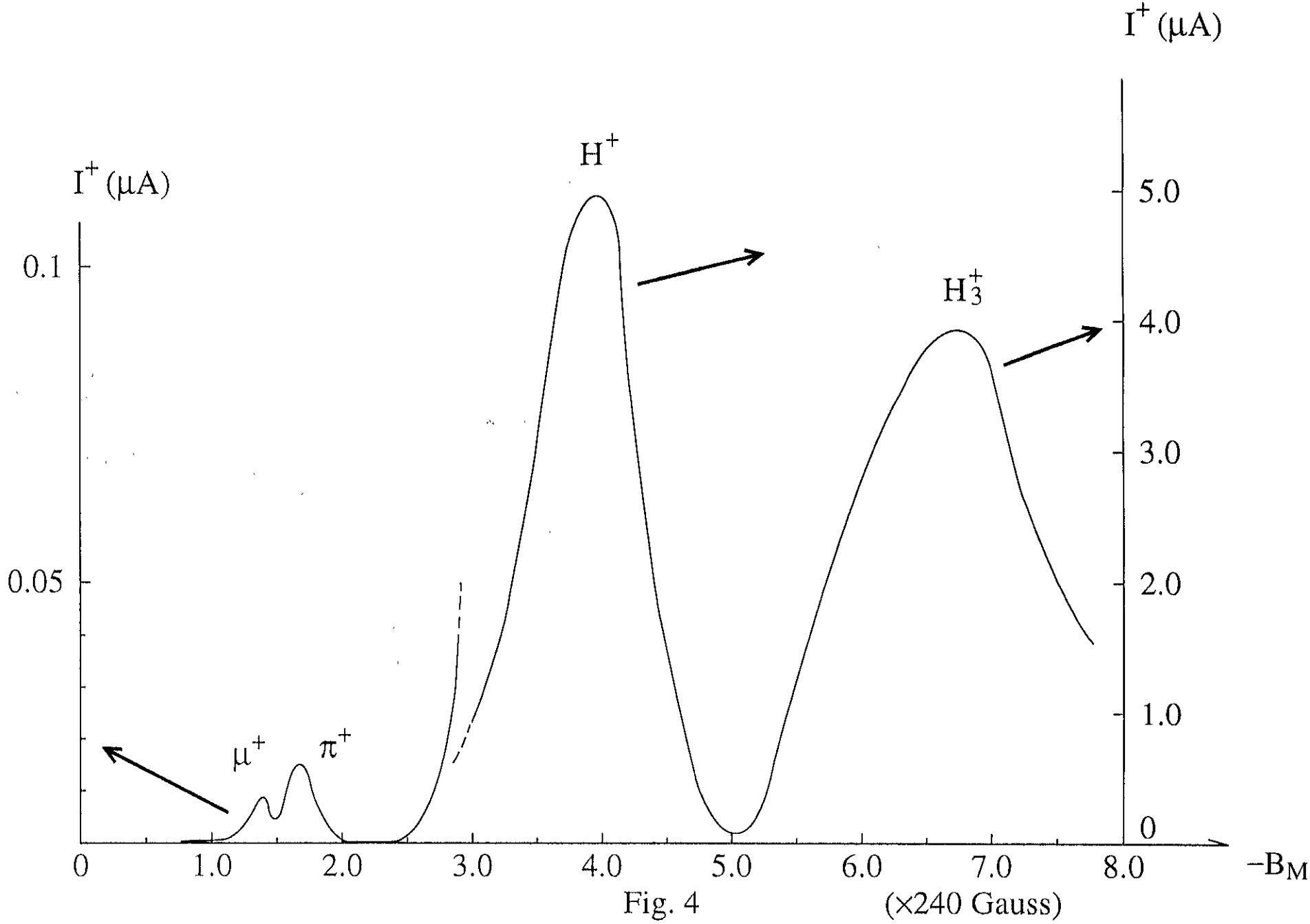
I+ (μA)
0.1
0.05
I+ (μA)
5.0
4.0
3.0
2.0
1.0
0
H+
H3+
μ+
π+
0
1.0
2.0
3.0
4.0
5.0
6.0
7.0
8.0
−BM
(×240 Gauss)

Fig. 4

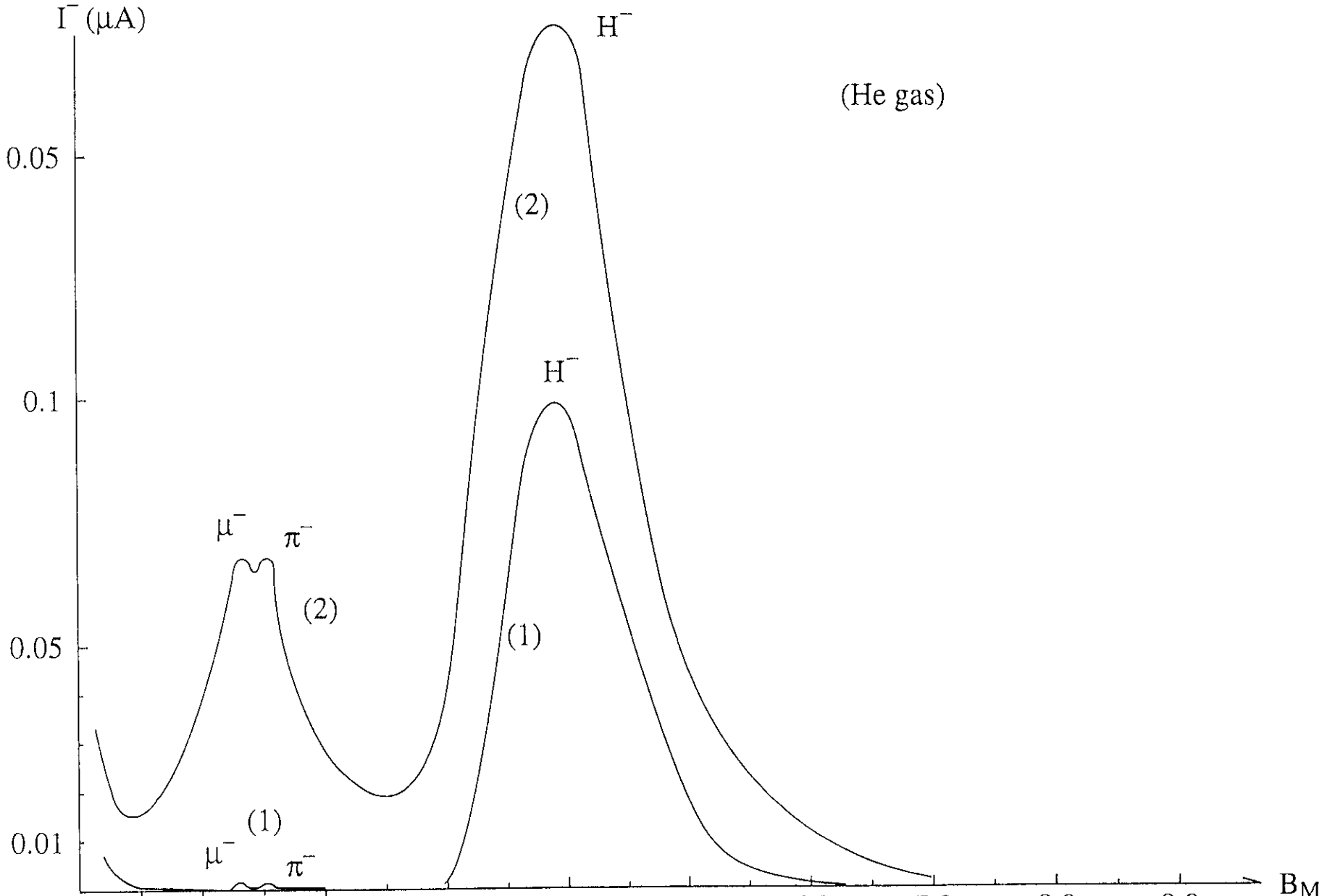
I⁻ (μA)
0.05
0.1
0.05
0.01
H⁻
(He gas)
(2)
H⁻
μ⁻
π⁻
(2)
(1)
(1)
μ⁻
π⁻
0
1.0
2.0
3.0
4.0
5.0
6.0
7.0
8.0
9.0
B_M
(×240 Gauss)

Fig. 5

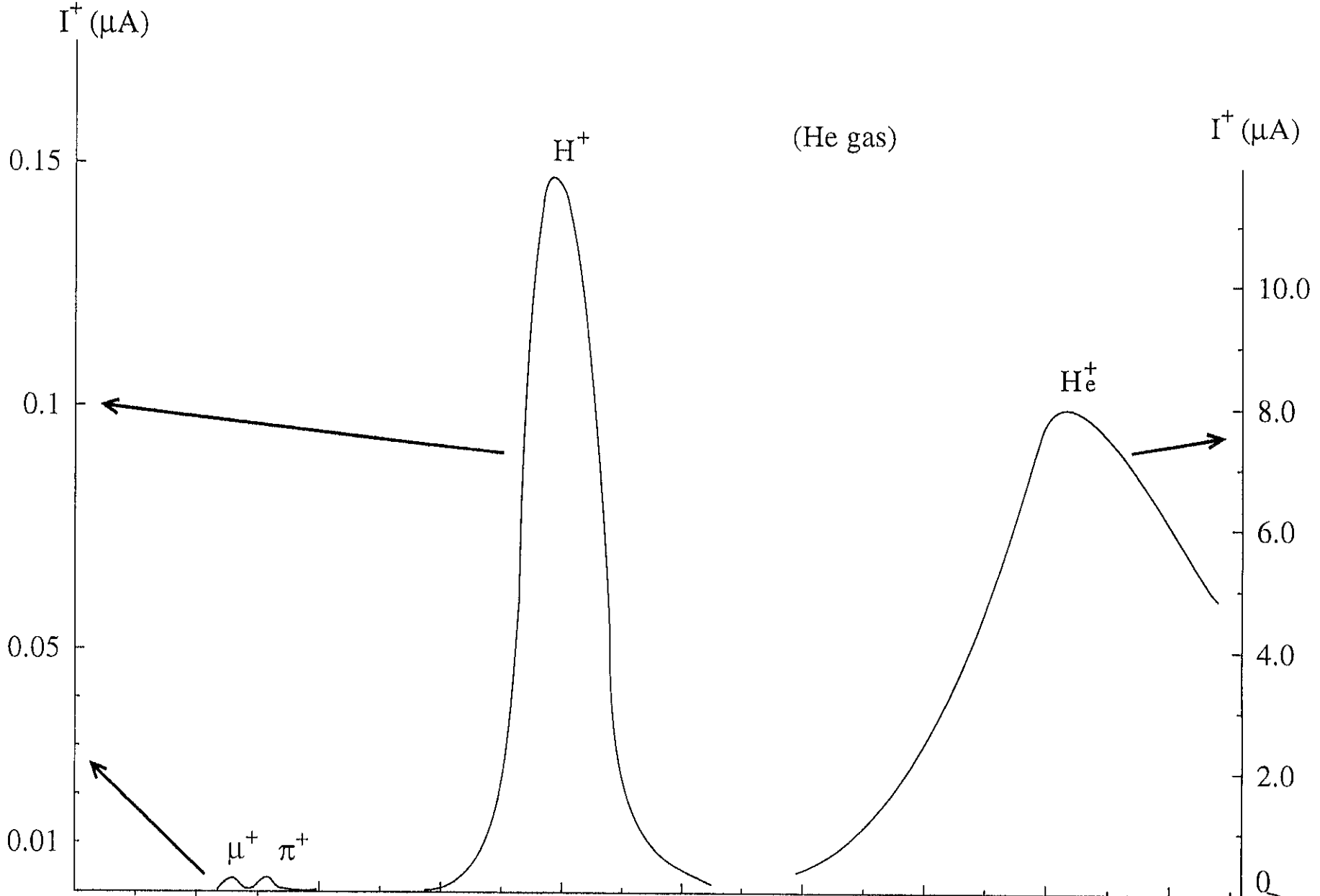
I+ (μA)
0.15
0.1
0.05
0.01
H+
(He gas)
I+ (μA)
10.0
8.0
6.0
4.0
2.0
0
He+
μ+ π+
0
1.0
2.0
3.0
4.0
5.0
6.0
7.0
8.0
9.0
−BM
(×240 Gauss)

Fig. 6

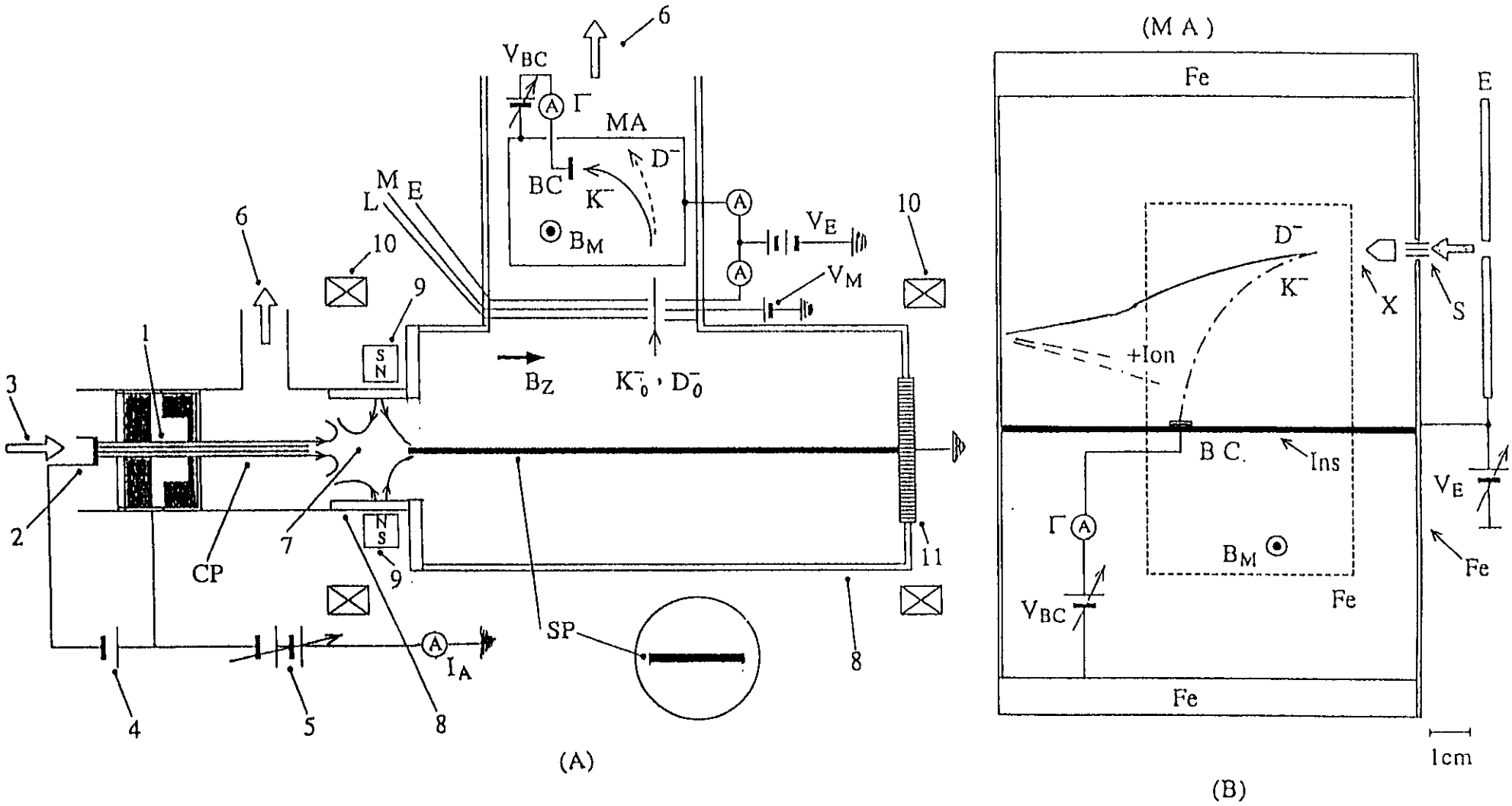
6
V_{BC}
Γ
MA
D^-
BC
K^-
M
L
E
B_M
V_E
V_M
10
9
1
3
2
CP
7
B_Z
K^-_0 , D^-_0
11
SP
8
I_A
4
5
(A)
(M A)
Fe
E
+Ion
X
S
B C.
Ins
B_M
Fe
1cm
(B)

Fig. 7

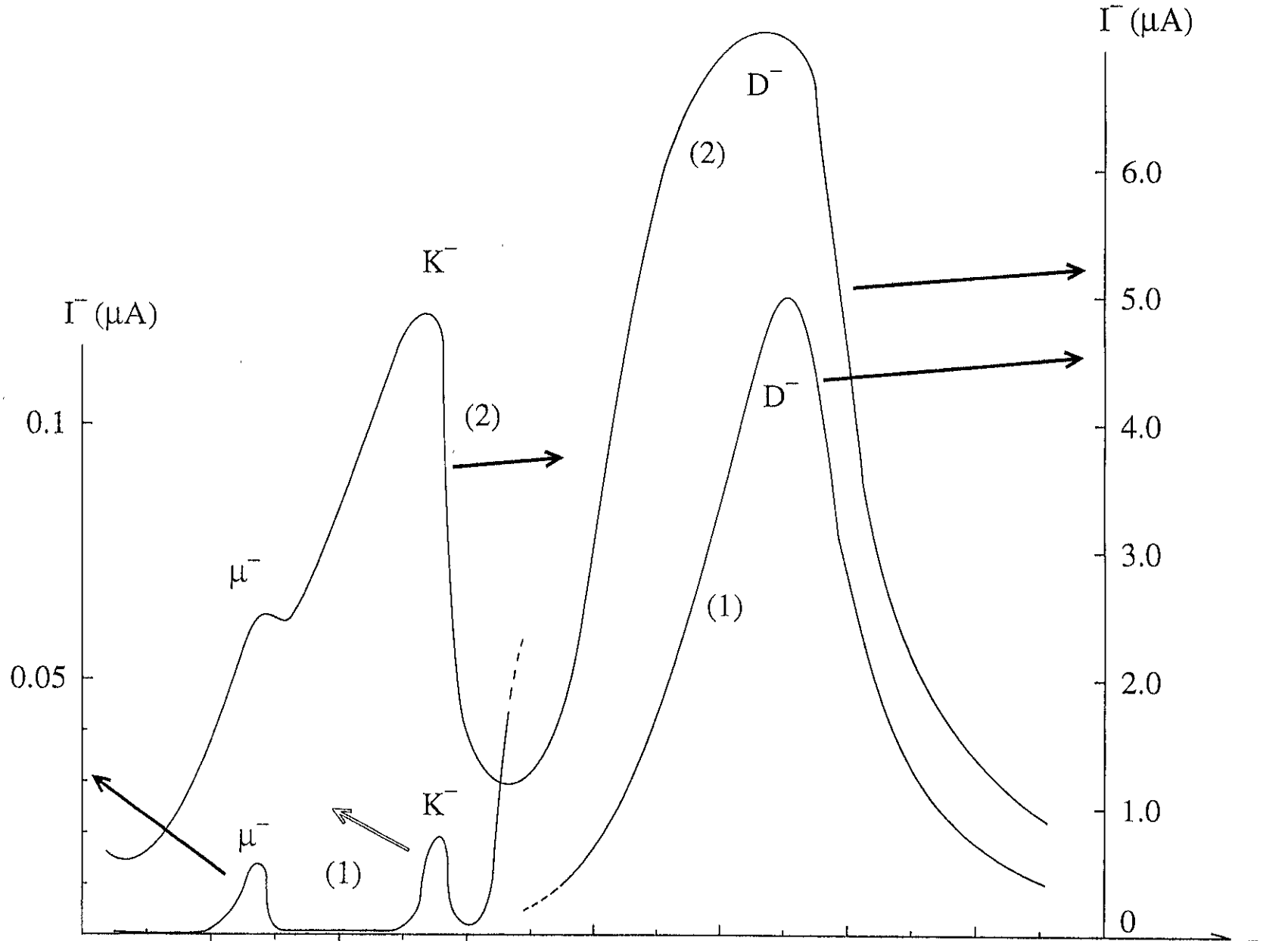
I⁻ (μA)
0.1
0.05
μ⁻
K⁻
(2)
(1)
μ⁻
K⁻
D⁻
(2)
D⁻
(1)
I⁻ (μA)
6.0
5.0
4.0
3.0
2.0
1.0
0
0
1.0
2.0
3.0
4.0
5.0
6.0
7.0
8.0
B_M
(×240 Gauss)

Fig. 8

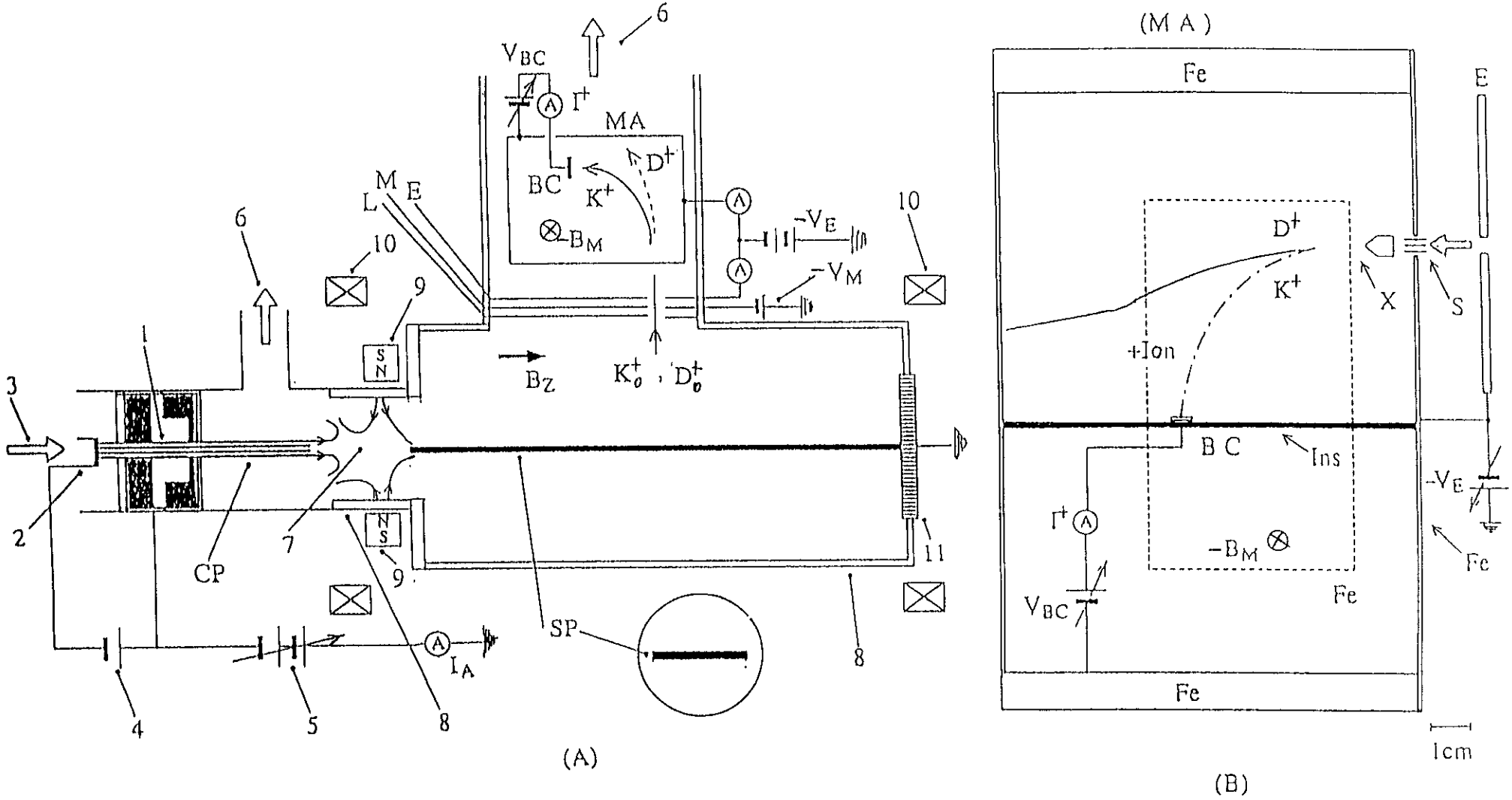
6
V_{BC}
I^+
MA
D^+
BC
K^+
B_M
M
L
E
$-V_E$
$-V_M$
10
9
B_Z
K_0^+ , D_0^+
3
1
2
CP
7
11
SP
8
I_A
4
5
(A)
(M A)
Fe
E
X
S
+Ion
BC
Ins
$-V_E$
Fe
$-B_M$
1cm
(B)

Fig. 9

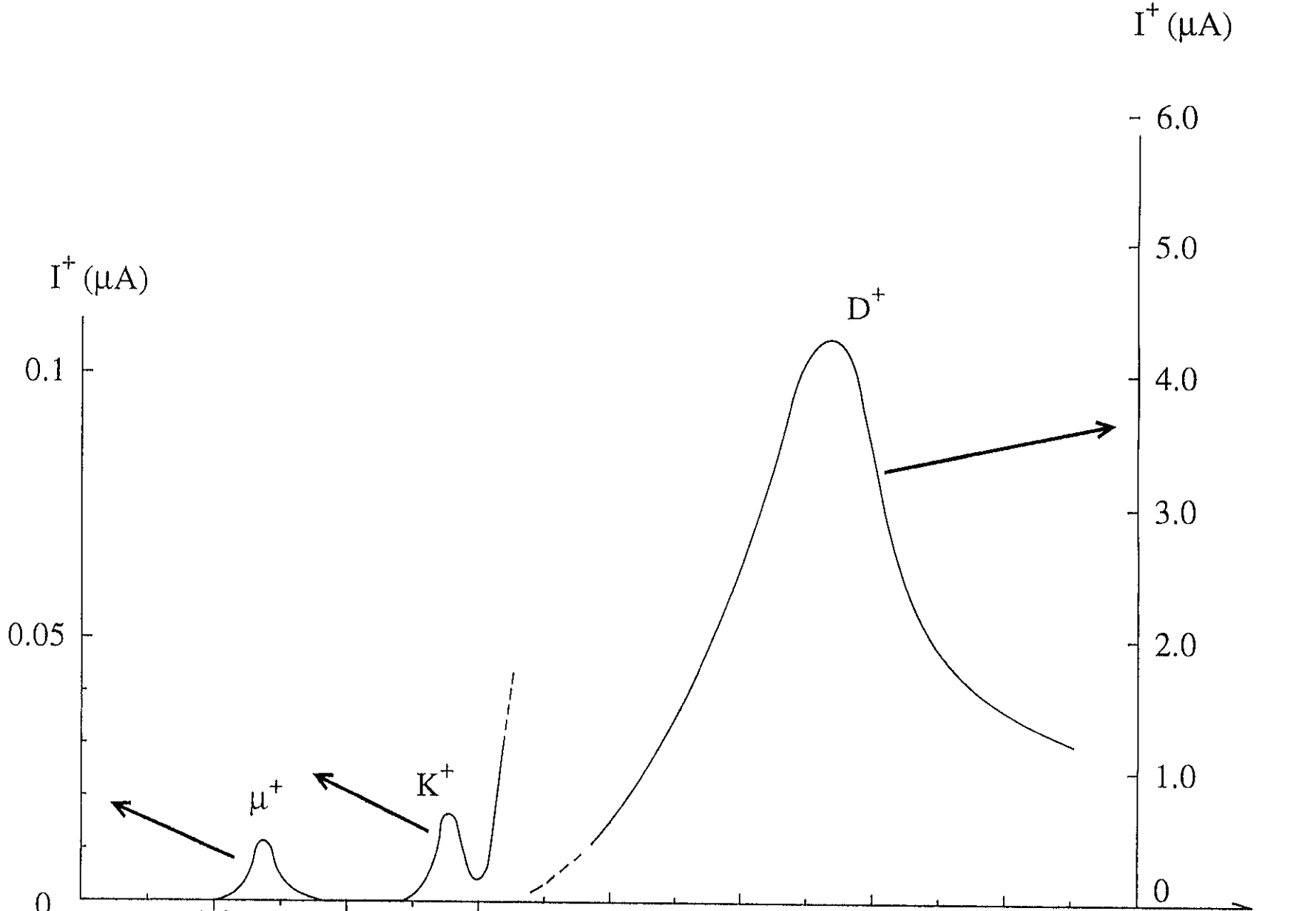
I+ (μA)
0.1
0.05
0
μ+
K+
D+
1.0
2.0
3.0
4.0
5.0
6.0
7.0
8.0
−BM
(×240 Gauss)
I+ (μA)
6.0
5.0
4.0
3.0
2.0
1.0
0

Fig. 10

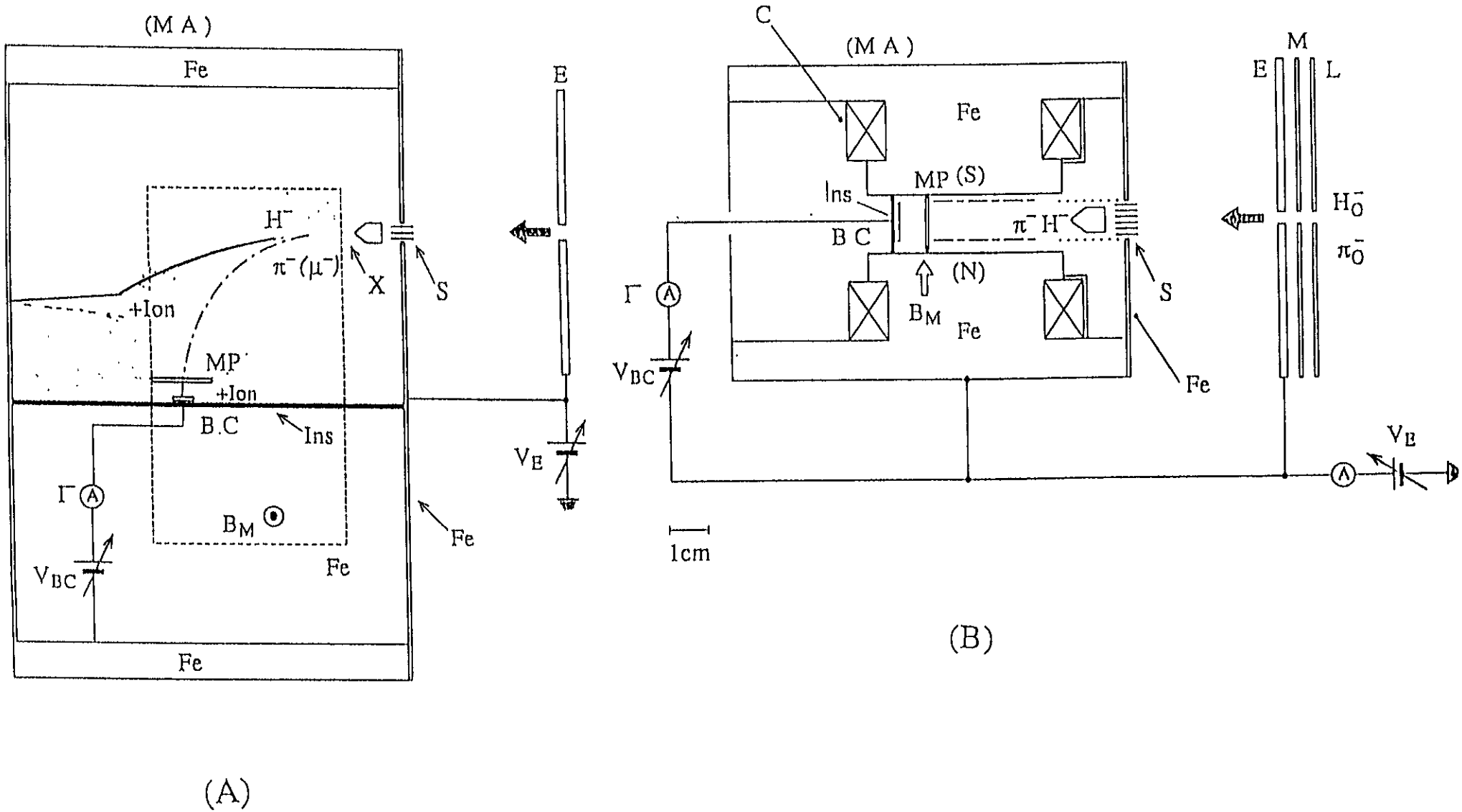
(M A)
Fe
E
H⁻
π⁻(μ⁻)
X
S
+Ion
MP
+Ion
B.C
Ins
Γ
A
B_M
V_BC
Fe
Fe
V_E
Fe
(A)
C
(M A)
Fe
MP (S)
Ins
B C
π⁻ H⁻
(N)
B_M
Fe
S
Γ
A
V_BC
Fe
M
E
L
H⁻O
π⁻O
V_E
A
1cm
(B)

Fig. 11

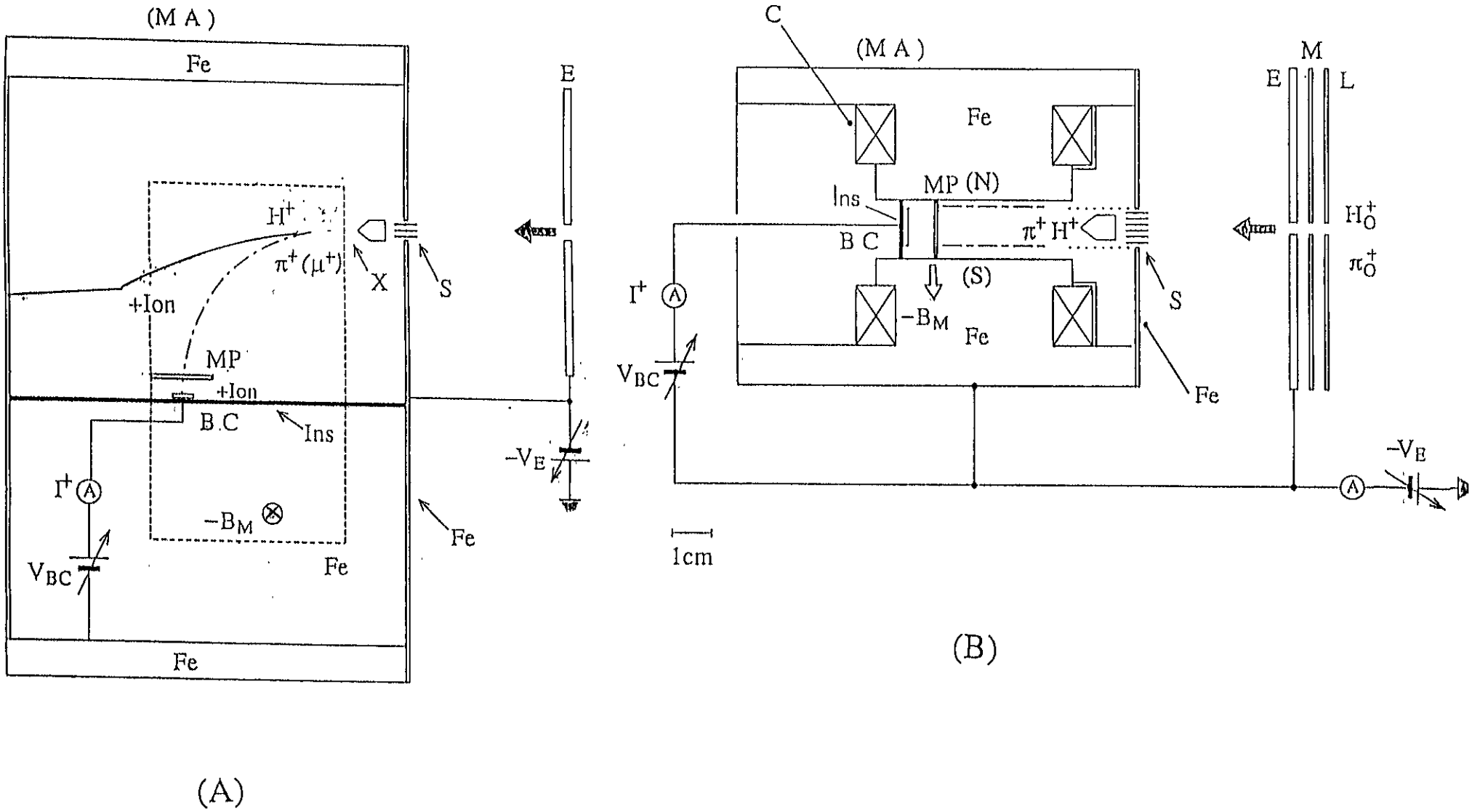
(M A)
Fe
E
H^+
$\pi^+(\mu^+)$
X
S
+Ion
MP
+Ion
B C
Ins
I^+
A
$-B_M$
V_{BC}
Fe
$-V_E$
Fe
Fe
(A)
C
(M A)
Fe
MP (N)
Ins
B C
π^+ H^+
(S)
I^+
A
$-B_M$
Fe
V_{BC}
S
Fe
M
E
L
H_O^+
π_O^+
$-V_E$
A
1cm
(B)

Fig. 12

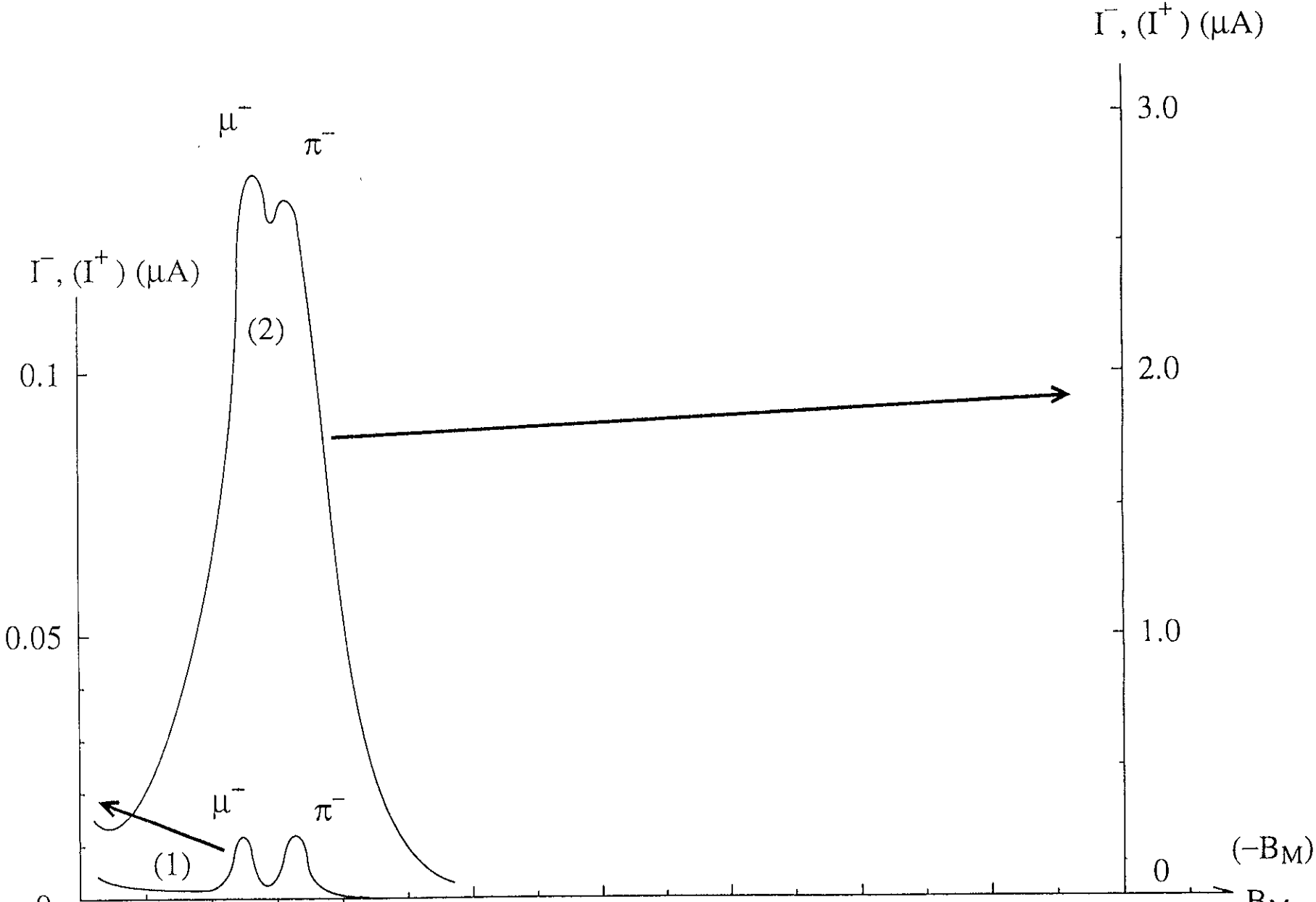

Fig. 13 (×240 Gauss)

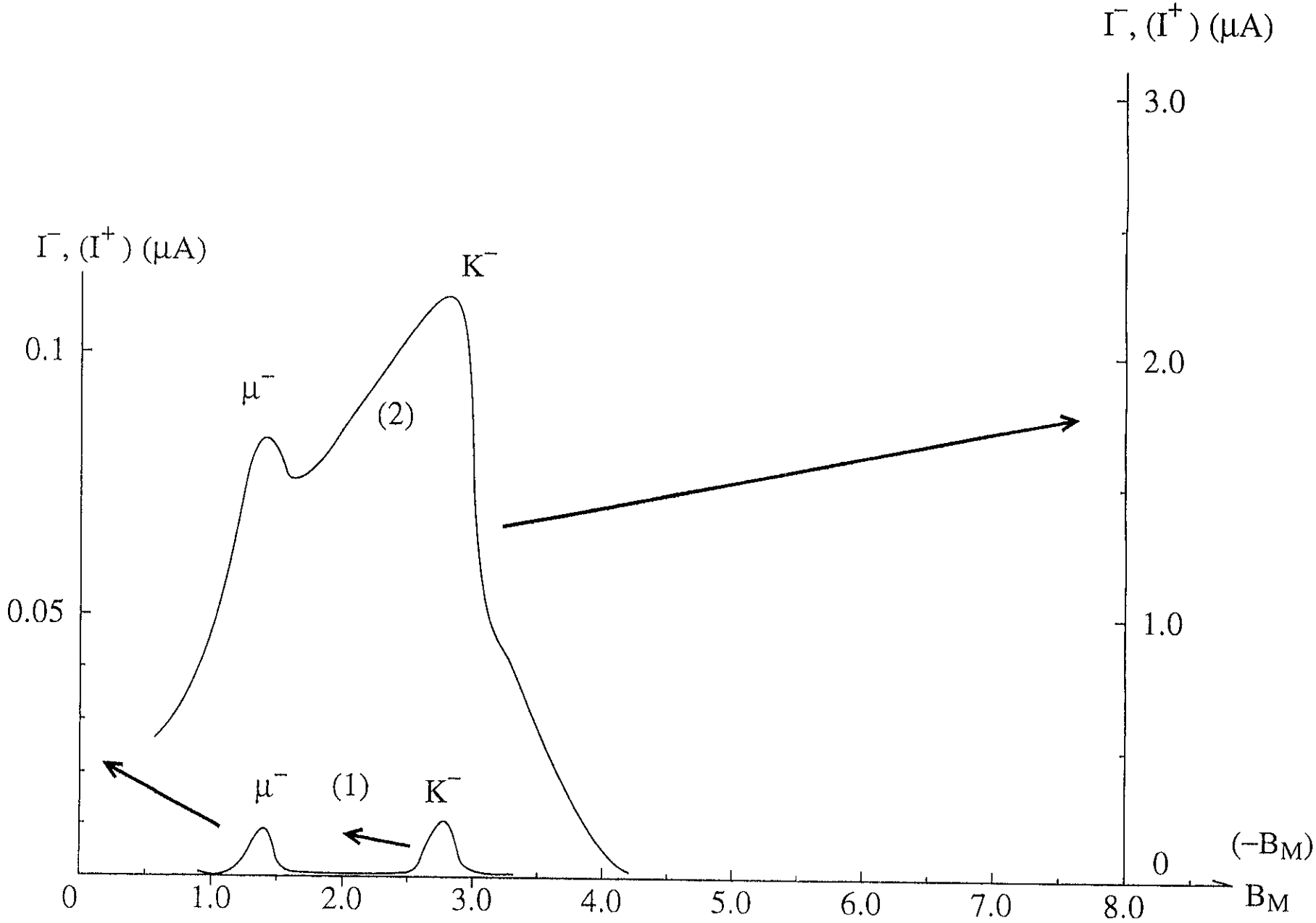
I⁻, (I⁺) (μA)
0.1
0.05
K⁻
μ⁻
(2)
μ⁻
(1)
K⁻
0
1.0
2.0
3.0
4.0
5.0
6.0
7.0
8.0
(×240 Gauss)
I⁻, (I⁺) (μA)
3.0
2.0
1.0
0
(−BM)
BM

Fig. 14

Recent Issues of NIFS Series

NIFS-493 S Ishiguro, T Sato, H Takamaru and The Complexity Simulation Group,
V-shaped dc Potential Structure Caused by Current-driven Electrostatic Ion-cyclotron Instability, May 1997

NIFS-494 K Nishimura, R Horiuchi, T Sato
Tilt Stabilization by Energetic Ions Crossing Magnetic Separatrix in Field-Reversed Configuration, June 1997

NIFS-495 T -H Watanabe and T Sato,
Magnetohydrodynamic Approach to the Feedback Instability, July 1997

NIFS-496 K Itoh, T Ohkawa, S -I Itoh, M Yagi and A Fukuyama
Suppression of Plasma Turbulence by Asymmetric Superthermal Ions, July 1997

NIFS-497 T Takahashi, Y Tomita, H Momota and Nikita V Shabrov
Collisionless Pitch Angle Scattering of Plasma Ions at the Edge Region of an FRC; July 1997

NIFS-498 M Tanaka, A Yu Grosberg, V S Pande and T Tanaka,
Molecular Dynamics and Structure Organization in Strongly-Coupled Chain of Charged Particles; July 1997

NIFS-499 S Goto and S Kida,
Direct-interaction Approximation and Reynolds-number Reversed Expansion for a Dynamical System; July 1997

NIFS-500 K Tsuzuki, N Inoue, A Sagara, N Noda, O Motojima, T Mochizuki, T Hino and T. Yamashina
Dynamic Behavior of Hydrogen Atoms with a Boronized Wall; July 1997

NIFS-501 I Vinar and S Sudo,
Multibarrel Repetitive Injector with a Porous Pellet Formation Unit; July 1997

NIFS-502 V Vdovin, T Watari and A Fukuyama,
An Option of ICRF Ion Heating Scenario in Large Helical Device, July 1997

NIFS-503 E. Segre and S Kida,
Late States of Incompressible 2D Decaying Vorticity Fields, Aug. 1997

NIFS-504 S Fujiwara and T. Sato,
Molecular Dynamics Simulation of Structural Formation of Short Polymer Chains, Aug 1997

NIFS-505 S Bazdenkov and T Sato
Low-Dimensional Model of Resistive Interchange Convection in Magnetized Plasmas, Sep 1997

NIFS-506 H Kitauchi and S Kida,
Intensification of Magnetic Field by Concentrate-and-Stretch of Magnetic Flux Lines, Sep 1997

NIFS-507 R L Dewar,
Reduced form of MHD Lagrangian for Ballooning Modes, Sep 1997

NIFS-508 Y -N Nejoh,
Dynamics of the Dust Charging on Electrostatic Waves in a Dusty Plasma with Trapped Electrons; Sep 1997

NIFS-509 E Matsunaga, T Yabe and M. Tajima,
Baroclinic Vortex Generation by a Comet Shoemaker-Levy 9 Impact; Sep 1997

NIFS-510 C C. Hegna and N Nakajima,
On the Stability of Mercier and Ballooning Modes in Stellarator Configurations, Oct. 1997

NIFS-511 K. Ohto and T. Hatori
Rotation and Oscillation of Nonlinear Dipole Vortex in the Drift-Unstable Plasma, Oct 1997

NIFS-512 J Uramoto
Clear Detection of Negative Pionlike Particles from H_2 Gas Discharge in Magnetic Field, Oct 1997

NIFS-513 T Shimozuma, M Sato, Y Takita, S Ito, S. Kubo, H Idei, K Ohkubo, T Watari, T S Chu, K. Felch, P Cahalan and C M Loring, Jr.

The First Preliminary Experiments on an 84 GHz Gyrotron with a Single-Stage Depressed Collector, Oct 1997

NIFS-514 T. Shimozuma, S Morimoto, M. Sato Y Takita S. Ito, S Kubo, H. Idei, K. Ohkubo and T Watari,
A Forced Gas-Cooled Single-Disk Window Using Silicon Nitride Composite for High Power CW Millimeter Waves; Oct. 1997

NIFS-515 K. Akaishi,
On the Solution of the Outgassing Equation for the Pump-down of an Unbaked Vacuum System: Oct. 1997

NIFS-516 *Papers Presented at the 6th H-mode Workshop (Seeon, Germany)*: Oct. 1997

NIFS-517 John L. Johnson,
The Quest for Fusion Energy, Oct. 1997

NIFS-518 J Chen, N Nakajima and M. Okamoto,
Shift-and-Inverse Lanczos Algorithm for Ideal MHD Stability Analysis; Nov 1997

NIFS-519 M. Yokoyama, N. Nakajima and M. Okamoto,
Nonlinear Incompressible Poloidal Viscosity in L=2 Heliotron and Quasi-Symmetric Stellarators; Nov. 1997

NIFS-520 S Kida and H Miura,
Identificaiton and Analysis of Vortical Structures· Nov. 1997

NIFS-521 K Ida, S Nishimura, T Minami, K. Tanaka, S. Okamura, M. Osakabe, H Idei, S. Kubo, C Takahashi and K. Matsuoka,
High Ion Temperature Mode in CHS Heliotron/torsatron Plasmas Nov. 1997

NIFS-522 M Yokoyama, N Nakajima and M. Okamoto,
Realization and Classification of Symmetric Stellarator Configurations through Plasma Boundary Modulations· Dec. 1997

NIFS-523 H. Kitauchi,
Topological Structure of Magnetic Flux Lines Generated by Thermal Convection in a Rotating Spherical Shell; Dec. 1997

NIFS-524 T. Ohkawa,
Tunneling Electron Trap; Dec. 1997

NIFS-525 K. Itoh, S.-I. Itoh, M. Yagi, A. Fukuyama,
Solitary Radial Electric Field Structure in Tokamak Plasmas; Dec. 1997

NIFS-526 Andrey N Lyakhov,
Alfven Instabilities in FRC Plasma, Dec 1997

NIFS-527 J. Uramoto,
Net Current Increment of negative Muonlike Particle Produced by the Electron and Positive Ion Bunch-method, Dec. 1997

NIFS-528 Andrey N. Lyakhov,
Comments on Electrostastic Drift Instabilities in Field Reversed Configuraiton; Dec. 1997

NIFS-529 J. Uramoto,
Pair Creation of Negative and Positive Pionlike (Muonlike) Particle by Interaction between an Electron Bunch and a Positive Ion Bunch; Dec. 1997

NIFS-530 J Uramoto,
Measuring Method of Decay Time of Negative Muonlike Particle by Beam Collector Applied RF Bias Voltage; Dec. 1997

NIFS-531 J. Uramoto,
Confirmation Method for Metal Plate Penetration of Low Energy Negative Pionlike or Muonlike Particle Beam under Positive Ions, Dec. 1997

NIFS-532 J. Uramoto,
Pair Creations of Negative and Positive Pionlike (Muonlike) Particle or K Mesonlike (Muonlike) Particle in H2 or D2 Gas Discharge in Magnetic Field; Dec. 1997